2018 European Control Conference (ECC)
June 12-15, 2018. Limassol, Cyprus

Minimization of steering corruption during front axle torque vectoring

Louis Filipozzi, Efstathios Velenis, and Francis Assadian

Abstract— **The effect of torque vectoring at the front steered axle on the steering torque is studied in this paper. A strategy is developed to implement front torque vectoring while preventing steering torque disturbances to the driver. This strategy is implemented in a Model Predictive Controller (MPC) based on a five degrees of freedom non-linear model. The controller provides optimal compromises between good yaw rate following performance and small steering torque corruption. The implementation of the strategy is compared against the passive vehicle and the unconstrained control cases using IPG CarMaker.**

I. Introduction

Car manufacturers have made great efforts in the development of hybrid and electric vehicles. They are indeed widely expected to be the transportation means for the future decades due to their low emissions. Beyond environmental friendliness, the electrification of vehicles has the potential to considerably improve handling characteristics thanks to the high controllability of electric motors and inclusion of multiple motors in the vehicle drivetrain.

Torque vectoring has been used in countless applications for safety and handling enhancement purposes. De Novellis [1] proposes to use Multiple Input Multiple Output (MIMO) controllers to regulate both the yaw rate and the sideslip angle of the vehicle to ensure safe driving. Similarly, Siampis [2] controls the yaw moment on the rear axle to stabilize the vehicle near the limit of lateral acceleration. Scheuch [3] suggests using torque vectoring in advanced driver assistance features like lane keeping system.

However, during front axle torque vectoring, the imbalance in longitudinal force generates a reaction torque on the steering wheel. In some situations, no alternatives to front axle torque vectoring are available, e.g. due to packaging constraints. And even, in the case of four wheels torque vectoring, the yaw moment generated by the front axle will create this undesired steering torque. Therefore, torque vectoring may alter the driver's steering feel. Moreover, Neukum and Krüger [4] show that varying the steering torque could result in a loss of control of the vehicle. The impact of torque vectoring on the steering feel has to be studied to ensure that the driver is providing unobstructed steering commands.

In this paper, we first investigate the effect of torque vectoring on the steering torque. Second, by treating the steering torque corruption as a torque disturbance, the driver's abilities to steer the vehicle during front torque vectoring are examined within the scope of a driver neuromuscular model developed by Cole [5]. Then, new requirements on the yaw moment controller are defined to ensure that the driver will not lose control of the vehicle. Finally, this constraint is implemented in a Model Predictive Control (MPC) framework and the new controller is tested with a high-fidelity vehicle model.

L. Filipozzi (corresponding author) and F. Assadian are with the Department of Mechanical and Aerospace Engineering, University of California, Davis, lfilipozzi@ucdavis.edu, and fassadian@ucdavis.edu. E. Velenis is with the Centre for Automotive Engineering, School of Aerospace, Transport and Manufacturing, Cranfield University, e.velenis@cranfield.ac.uk.

II. Impact of torque vectoring on the steering feel

A. Estimation of the steering torque corruption

The steering torque felt by the driver results from the moment generated by the interaction forces between the tires and the road around the kingpin axis. In addition to this torque, damping and inertia in the steering system also contribute to the handwheel torque [6].

In conventional vehicles, the main contribution to the steering torque is made by the lateral forces [7]. However, with torque vectoring on the front axle, the contribution of longitudinal force to the steering torque can considerably change the steering feel. Considering the front left wheel, the contribution of its tractive force F_{FLx} is:

$$M_{corr,L} = \frac{(s_r \cos\lambda + r \sin\lambda)\cos\nu F_{FLx}}{i_{steer}} \tag{1}$$

where s_r is the scrub radius, r denotes the wheel radius, λ the lateral kingpin inclination, ν the caster angle, and i_{steer} the steering ratio. The lever arm $(s_r \cos\lambda + r \sin\lambda)\cos\nu$ corresponds to the kingpin offset at the wheel hub.

Since the moments generated by the left and right wheel on the kingpin axis are opposite, the total torque is:

$$M_{corr} = -M_{corr,L} + M_{corr,R} \tag{2}$$

$$= \frac{(F_{FRx} - F_{FLx})(s_r \cos\lambda + r \sin\lambda)\cos\nu}{i_{steer}} \tag{3}$$

The yaw moment M_z generated by torque vectoring is also linked to the imbalance in longitudinal force. If the center of mass is assumed to be at the middle of the car in the lateral direction, the yaw moment is $M_z = (F_{FRx} - F_{FLx})w/2$ where w is the vehicle width. Therefore, if we consider only the contribution of the longitudinal term, the handwheel torque corruption due to torque vectoring is:

$$M_{corr} = \frac{2(s_r \cos\lambda + r \sin\lambda)\cos\nu}{i_{steer} w} M_z \tag{4}$$

Consequently, with a relative understeer target, torque vectoring counters the yaw rotation of the vehicle and a centering effect is added in the steering system. The driver has

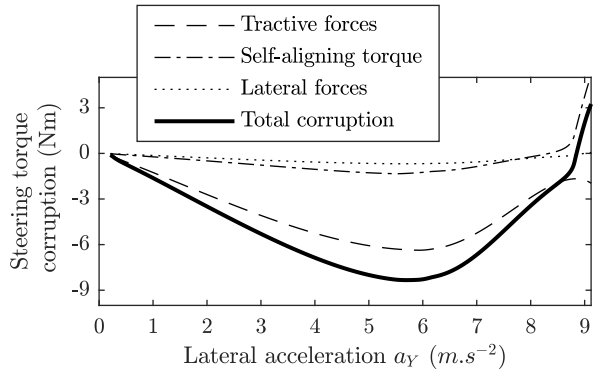

Fig. 1. Contribution of lateral, longitudinal forces and self-aligning moment to the steering torque corruption due to torque vectoring

to deliver a higher torque to make the turn. On the contrary, with a relative oversteer target, the yaw moment assists the yaw rotation of the vehicle. The steering torque corruption lowers the steering torque the driver has to provide. In both situations, torque vectoring change the steering feel of the vehicle.

B. Verification

Equation (4) has been checked against a simulation run in MATLAB environment with a five degrees of freedom double-track model (Section IV-A). The simulation consists in a constant steering angle maneuver (ISO 4138:2012). Rolling resistance and overturning moment are not considered since their projections on the kingpin axis are second-orders [7]. The variation of the suspension geometry due to bump and rebound is neglected. Longitudinal and lateral forces and self-aligning moment are computed utilizing Pacejka's Magic Formula [8].

A vehicles with a torque vectoring controller who aims to achieve an understeer gradient $K_U = 2\,\mathrm{deg\,g}$ are tested (Section IV-B). The contribution of longitudinal, lateral, and the self-aligning moment on the steering torque have been computed and compared with those of a passive vehicle for the same lateral acceleration yielding a map of the steering torque corruption versus the lateral acceleration. Figure 1 provides the contribution of each term to the steering torque corruption for two understeer gradients K_U.

The torque corruption due to tractive forces is largely responsible for the steering torque corruption. However, the corruption due to self-aligning torque may be non-negligible, especially at the limit of lateral acceleration. The estimation of the corruption through Equation (4) underestimates the total corruption. However, due to the simplicity of the equation, it is used in the following of this paper.

III. Driver's abilities to steer the vehicle

A. Neuromuscular model

To understand the driver's reaction to torque disturbance and to help with the design of a new torque vectoring strategy, Cole's neuromuscular model has been used [5], [9]. It features co-contraction and reflex. Co-contraction (itshape

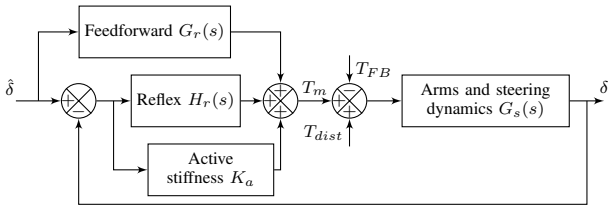

Fig. 2. Cole's linear neuromuscular model of the driver featuring co-activation and reflex [5]

"Active stiffness" block) refers to the simultaneous activation of both agonist and antagonist muscles. These two processes have been identified by Abbink [10] as two major and effective mechanisms to reject torque perturbations during the steering task. Moreover, Sharp's path following controller is implemented to account for closed-loop maneuvers [11].

The neuromuscular model is illustrated in Figure 2. The *"Arms and steering dynamics"* bloc models the interaction between the driver and the steering wheel. Its transfer function $G_s(s)$ is a second order which accounts for inertia, a compliance and a damper. Cole provides values for this parameters [5]. In the following, inertia, damping and stiffness are respectively set to $J = 0.27\,\mathrm{kg\,m^2}$, $B = 1.54\,\mathrm{N\,m\,s\,rad^{-1}}$, and $K = 6.09\,\mathrm{N\,m\,rad^{-1}}$.

$$G_s(s) = \frac{1}{Js^2 + Bs + K} \tag{5}$$

The feedforward block $G_r(s)$ delivers the torque the driver has to provide in order to achieve the desired steering angle $\hat{\delta}$. It symbolizes the past experience of the driver with the steering task. Ideally, $G_r(s)$ is defined such that without external disturbance, the steering angle desired by the driver $\hat{\delta}$ matches perfectly the obtained steering angle δ.

$$G_r(s) = \frac{1 + G_s(s)P(s)}{G_s(s)} \text{ where } P(s) = \frac{1}{i_{steer}} \frac{T_{FB}(s)}{\Delta(s)} \tag{6}$$

$P(s)$ is the transfer function between the effective steering angle δ and the torque feedback T_{FB} provided to the driver from lateral forces. To obtain $P(s)$, the vehicle is represented by a bicycle model whose velocity is $10\,\mathrm{m\,s^{-1}}$.

The active stiffness block which represents the increase in the muscle stiffness during co-contraction is a gain set to $K_a = 60\,\mathrm{N\,m\,rad^{-1}}$. The reflex control $H_r(s)$ is described as a phase-lead compensator with time delay $\tau_r = 0.04\,\mathrm{s}$. T_m is the torque supplied by the driver on the steering wheel. T_{dist} is a torque disturbance injected in the steering system. In the following of the paper, T_{dist} is the torque corruption generated by torque vectoring. For more information about the neuromuscular model, the reader should refer to [5].

B. Disturbance shape analysis

The aim of this section is to determine conditions on the torque disturbance that will not impede the steering task. The reaction of a driver is studied with Cole's neuromuscular model for two shapes: a ramp and a step. The tested disturbances are a step or a ramp for $15\,\mathrm{s}$ and then a ramp down as shown in Figure 3a. The driver aims to maintain the

vehicle on a straight line. Without torque disturbance $\hat{\delta} = 0$ in Figure 2, thus, the steering angle deviation corresponds to the output δ of the neuromuscular model. As illustrated in Figure 3b, a step disturbance causes large deviation in the steering angle. But, the driver is able to withstand slow ramps of torque disturbance.

In [12], Switkes *et al.* conducted experiments in which the steering system was submitted to ramp or step torque disturbances. Their results are similar to those obtained with the neuromuscular model. More precisely, the delay between the occurrence of the disturbance and the time at which the maximum steering wheel deviation occurs is found to be independent of the disturbance amplitude. Moreover, the maximum handwheel deviation is proportional to the amplitude with step disturbances. But, it depends on the ramp rate for ramp disturbances. Such properties show that a linear model is sufficient to describe the driver.

To conclude, the shape of the disturbance has a major impact on the driver's threshold of perception. The driver is able to reject large disturbance torque as long as the disturbance is increased slowly. To prevent torque vectoring from disturbing the driver, the torque disturbance must respect a rate constraint ΔM_{corr}. Moreover, Equation (4) provides a linear relation between the yaw moment and the steering torque. Therefore, the rate constraint on the yaw moment is:

$$\Delta M_z = \frac{i_{steer} w}{2(s_r \cos\lambda + r \sin\lambda)\cos\nu} \Delta M_{corr} \tag{7}$$

IV. Vehicle model and reference

A. Five degrees of freedom vehicle model

The vehicle is represented by a four-wheel model. Rear wheels are assumed to be free-rolling. The equations of motion are [2]:

$$\begin{aligned} m\dot{v} = &(F_{FLx} + F_{FRx})\cos(\delta - \beta) \\ &- (F_{FLy} + F_{FRy})\sin(\delta - \beta) \\ &+ (F_{RLy} + F_{RRy})\sin\beta \end{aligned} \tag{8}$$

$$\begin{aligned} \dot{\beta} = &\frac{1}{mv}[(F_{FLx} + F_{FRx})\sin(\delta - \beta) \\ &+ (F_{FLy} + F_{FRy})\cos(\delta - \beta) \\ &+ (F_{RLy} + F_{RRy})\cos\beta] - \dot{\psi} \end{aligned} \tag{9}$$

$$\dot{\omega}_{Fj} = (T_{Fj} - F_{Fjx} r)/I_w, \quad j = L, R \tag{10}$$

$$\begin{aligned} I_{zz}\ddot{\psi} = &l_F[(F_{FLy} + F_{FRy})\cos\delta \\ &+ (F_{FLx} + F_{FRx})\sin\delta] - l_R(F_{RLy} + F_{RRy}) \\ &+ w_L(F_{FLy}\sin\delta - F_{FLx}\cos\delta) \\ &+ w_R(F_{FRx}\cos\delta - F_{FRy}\sin\delta) \end{aligned} \tag{11}$$

where m is the mass of the vehicle, I_{zz} is its moment of inertia around the vertical axis, v is the velocity of the vehicle's center of mass, β is the sideslip angle, r denotes the wheel radius, l_F (resp. l_R) is the distance between the front axle (resp. the rear axle) and the center of mass, and w_L (resp. w_R) is the lateral distance between the left wheel (resp. the right wheel) and the center of mass. We set $w_L = w_R$ so that the center of mass is in the center of the vehicle with respect to the lateral axis.

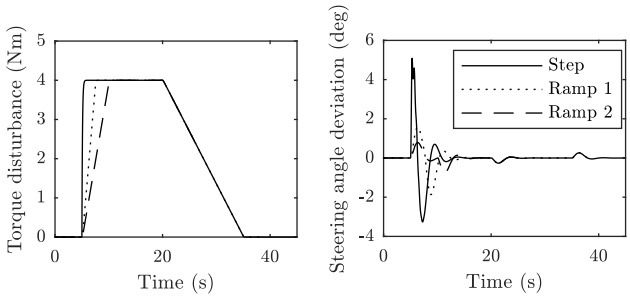

(a) (b)

Fig. 3. Impact of disturbance shape on the driver reaction

The yaw moment M_z and the total torque T_{tot} applied on the vehicle are defined by:

$$T_{tot} = T_{FL} + T_{FR} \text{ and } M_z = \frac{w_R}{r} T_{FR} - \frac{w_L}{r} T_{FL} \tag{12}$$

Longitudinal and lateral tire slip s_{ijx} and s_{ijy} provide the resultant tire slip $s_{ij} = \sqrt{s_{ijx}^2 + s_{ijy}^2}$. The combined friction coefficient is obtained from a simplified Pacejka's magic formula. Lateral and longitudinal friction coefficients are computed assuming a friction circle map. Tire forces are then given by (15). The vertical load F_{ijz} is based on the algebraic load and the longitudinal and lateral weight transfer due to acceleration. The pitch and roll motion of the vehicle sprung mass are neglected.

$$\mu_{ij}(s_{ij}) = \mathrm{MF}(s_{ij}) = D\sin(C\tan^{-1}(Bs_{ij})) \tag{13}$$

$$\mu_{ijx} = -\frac{s_{ijx}}{s_{ij}}\mu_{ij}(s_{ij}), \quad \mu_{ijy} = -\frac{s_{ijy}}{s_{ij}}\mu_{ij}(s_{ij})l \tag{14}$$

$$F_{ijx} = \mu_{ijx} F_{ijz}, \quad F_{ijy} = \mu_{ijy} F_{ijz} \tag{15}$$

B. Reference generation

De Novellis *et al.* [13] provide the design of a reference generator which aims to maintain a parameterizable understeer gradient K_U independently of the vehicle speed up to the lateral acceleration a_Y^*. To yield the reference yaw rate, the ratio K_s between the steering angle and lateral acceleration has to be defined:

$$K_s = \frac{l + K_U v^2}{v^2} \tag{16}$$

The reference yaw rate is obtained from (17) and (18).

$$\dot{\psi}_{ref} = \frac{a_{Y,ref}}{v} \tag{17}$$

$$a_{Y,ref} = \begin{cases} \frac{\delta}{K_s} & \text{if } \delta < a_Y^* K_s \\ a_{Y,max} + (a_Y^* - a_{Y,max}) e^{\frac{a_Y^* K_s - \delta}{(a_{Y,max} - a_Y^*)K_s}} & \text{if } \delta \geq a_Y^* K_s \end{cases} \tag{18}$$

where $a_{Y,max}$ is the maximum lateral acceleration achievable and a_Y^* is the maximum lateral acceleration in the region of the understeer characteristic which has been set to $0.6\ a_{Y,max}$.

To supply reference value for other state variables, a steady-state analysis is conducted. Under steady-state condition, Equations 8 to 15 form a system whose unknowns are $(v, \beta, \dot{\psi}, \omega_{FL}, \omega_{FR}, T_{tot}, M_z, \delta)$ and which requires three unknowns as inputs to be solved. The triplet $(\dot{\psi}_{ref}, \delta, v)$ is given to obtain the desired yaw behavior under steady-state. The problem is solved by MATLAB non-linear solver `fsolve` and saved into look-up tables. The reference value $x_{ref} = \begin{bmatrix} v & \beta_{ss} & \dot{\psi}_{ref} & \omega_{FL,ss} & \omega_{FR,ss} \end{bmatrix}^T$ and $u_{ref} = \begin{bmatrix} M_{z,ss} & T_{tot,ss} & \delta \end{bmatrix}^T$ are then obtained on-line by linear interpolation around the triplet $(\dot{\psi}_{ref}, \delta, v)$.

V. MPC PROBLEM

An MPC formulation features a discrete internal model of the system it controls. The non-linear five degrees of freedom model described in Section IV-A with state vector x and input u is used: $\dot{x} = f(x, u)$. This system is linearized off-line about the same breakpoints used for the steady-state analysis and then discretized using `c2d` MATLAB function with zero-order hold method. Discrete state matrices A_{bp}, B_{bp}, C_{bp} and D_{bp} are stored into look-up tables to maintain the computational burden law and to allow implementation of the controller.

At each timestep i, the MPC solve an optimization problem:

$$\text{minimize } \mathcal{J} = \tilde{x}_{N_p}^T P \tilde{x}_{N_p} + \sum_{k=0}^{N_p-1} \tilde{x}_k^T Q \tilde{x}_k + \tilde{u}_k^T R \tilde{u}_k \quad (19)$$

$$\text{subject to } \tilde{x}_{k+1} = A\tilde{x}_k + B\tilde{u}_k \quad (20)$$

$$u_{min} \leq u_k \leq u_{max} \quad (21)$$

$$\Delta u_{min} \leq \Delta u_k = u_k - u_{k-1} \leq \Delta u_{max} \quad (22)$$

where $\tilde{x}_k = x_k - x_{k,ref}$ is the difference between the vehicle states and the reference states, and $\tilde{u}_k = u_k - u_{k,ref}$ is the difference between the current input and the reference input at timestep k of the receding horizon.

The MPC minimizes the cost function $\mathcal{J}$, a quadratic error between the reference and measured values. Weight matrices Q and R are diagonals matrices whose coefficient are scale factors used to normalize the problem.

Equation (20) is the dynamic model of the system. Matrices A and B are obtained after linear interpolation of matrices A_{bp} and B_{bp} stored into look-up tables. They are the Jacobian matrices from linearization around the vehicle performing point at timestep i. Constraints on the maximum yaw moment achievable due to motor torque limit are taken into account in (21). Finally, Equation (22) implements the rate constraint on the steering torque corruption as discussed in Section III-B. There is no constraint on the rate of the other inputs: i.e., T_{tot} and δ.

A. Parameter tuning

Two major tuning parameters of an MPC are the sampling time T_s and the prediction horizon T_p. They result from a trade-off between the computational burden and the tracking performance. The time required to solve the optimization problem at each timestep is provided by the solver: FORCES Pro [14]. The mean computational time is used to evaluate the need for computational resources. Performance is evaluated with the integral quadratic error $\mathcal{E}$ between the reference and the actual input and output of the plant over the entire simulation duration T (not only over the prediction window of the MPC) with the simulation sampling time $T_{s,sim} = 1\,\text{ms}$.

$$\mathcal{E} = \sum_{i=1}^{\lfloor T/T_{s,sim} \rfloor} (\tilde{x}^T[i] Q \tilde{x}[i] + \tilde{u}^T[i] R \tilde{u}[i]) T_{s,sim} \quad (23)$$

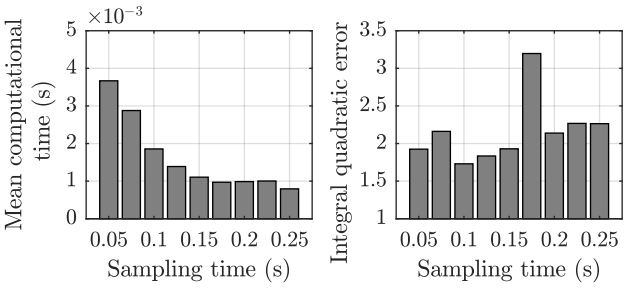

(a) Variation of the sampling time T_s with $T_p = 5.0\,\text{s}$

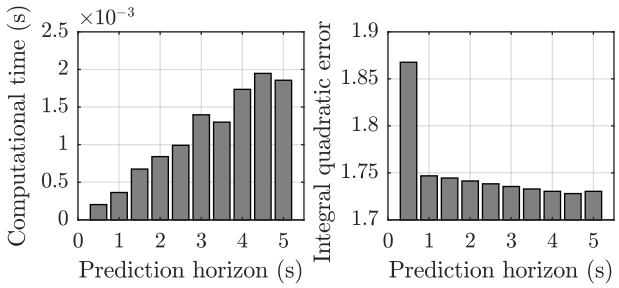

(b) Variation of the prediction horizon T_p with $T_s = 0.1\,\text{s}$

Fig. 4. Tuning of the MPC parameters T_s and T_p. The simulation test is a step steering input with $\delta = 3°$, $K_U = 2\,\text{deg/g}$. The simulation duration is $T = 5\,\text{s}$.

First, the effect of varying the sampling time is investigated. The simulation corresponds to a step steer test with $\delta = 3°$. The prediction horizon is set to the duration of the simulation, i.e. $T_p = N_p T_s = 5\,\text{s}$. The results are given in Figure 4a. A coarser sampling time reduced the computational burden at the expense of the performance of the system. A sampling time of $0.1\,\text{s}$ shows a good compromise between computational burden and the integral quadratic error $\mathcal{E}$.

Then, the prediction horizon is varied. Result are given in Figure 4b. Reducing the prediction horizon decreases the number of variables handled by the controller and therefore, the time required to solve the optimization problem. Though, it decreases the performance too. Nevertheless, the simulation shows very little variation of the performed cost when $T_p \geq 1\,\text{s}$. The prediction horizon is set to $T_p = 1.0\,\text{s}$.

To further reduce the need for computational resources, the control horizon could be shortened to limit the number of variable in the optimization problem. But this has not been examined.

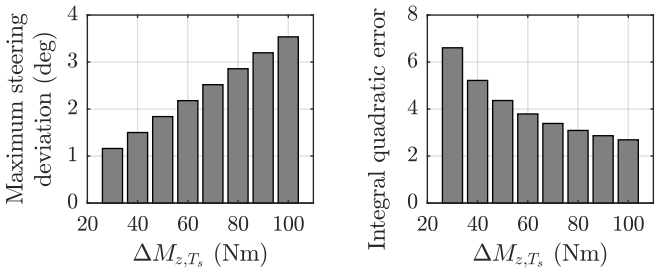

Fig. 5. Trade-off between handling performance and corruption minimization.

B. Study of the rate constraint

To minimize the steering corruption with an optimal controller, the approach of this paper focuses on the implementation of the rate constraint on the yaw moment. The outcomes resulting from this rate constraint have to be investigated.

To study the performance of the closed-loop system, the five degrees of freedom model is used to perform a step maneuver with a steering step $\delta = 5°$, and an initial speed $v = 50\,\mathrm{km\,h^{-1}}$. The torque vectoring controller aims to achieve the understeer target $K_U = 2\,\mathrm{deg/g}$. To study the minimization of the steering corruption, the torque disturbance produced by the yaw moment is fed into Cole's neuromuscular model. This simulation is repeated for several values of $\Delta M_{z,T_s} = M_z(t+T_s) - M_z(t)$ and the results are shown in Figure 5.

As it can be seen, a low yaw moment rate leads to a small steering angle deviation. The linearity of this relation is due to the linearity of the neuromuscular model. On the contrary, the integral quadratic error decreases when the rate constraint increases since the vehicle takes more time to reach steady-state. The choice of the limit value for the yaw moment rate results from a trade-off between the performance of the torque vectoring system and the minimization of the steering corruption. A limit value of $80\,\mathrm{N\,m}$ is chosen in order to keep reasonable performance. From Equation (7) and $\Delta M_z = \Delta M_{z,T_s}/T_s$, it corresponds to a steering torque disturbance rate of $4\,\mathrm{N\,m\,s^{-1}}$.

C. High-fidelity validation

In this section, the MPC controller is validated against a high-fidelity software: CarMaker. It allows the use of a high fidelity model of the vehicle and the simulation of closed-loop test. The scenario consists in a straight line of $40\,\mathrm{m}$ followed by a hairpin turn whose constant radius is $40\,\mathrm{m}$. The vehicle is first driven on a $50\,\mathrm{m}$ straight line with a $80\,\mathrm{km\,h^{-1}}$ initial speed. The vehicle then takes the left U-turn. Finally, the vehicle is driven in a straight line again. Torque vectoring enforces an understeer target $K_U = 2\,\mathrm{deg/g}$. The road coefficient is set to $\mu_{road} = 1$. With these conditions, at the middle of the turn, the vehicle is close to the limit of lateral acceleration.

The MPC is compared with a Linear Quadratic Regulator (LQR) whose cost parameters are the same (Figure 6). The

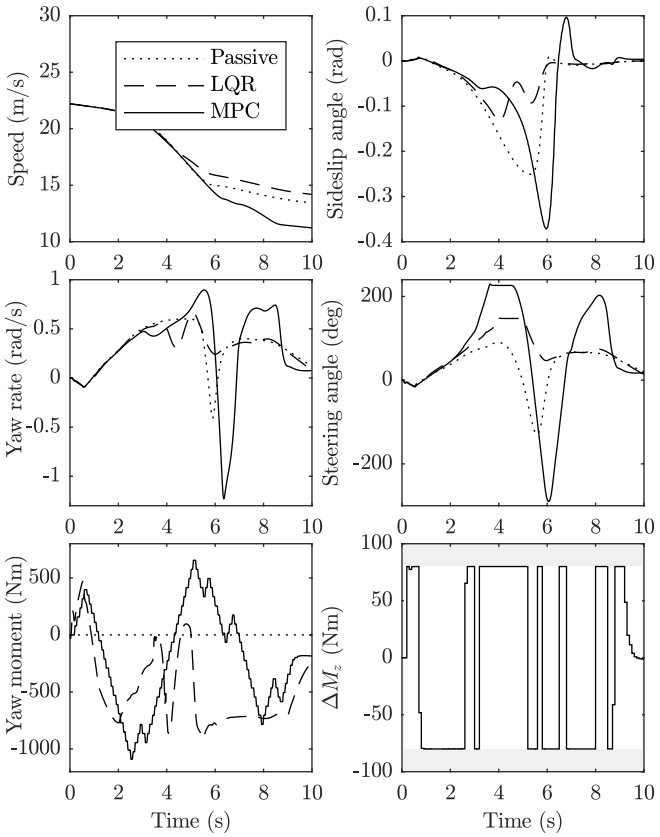

Fig. 6. Result from hairpin turn with hard constraints. The dotted lines stand for the passive vehicle, the solid ones for the LQR controlled vehicle and the dashed ones for the MPC controlled vehicle.

LQR provide good result. The vehicle is more understeering over the entire turn. But with this controller, there is no steering corruption minimization.

During the first half of the turn, the MPC provides satisfactory results. However, at $t = 5\,\mathrm{s}$, the yaw moment should suddenly drop to minimize the sideslip angle and keep the vehicle stability. Due to the restriction on the yaw moment rate, such a variation is not possible. Therefore, torque vectoring enforces a relative oversteer behavior when it should be a relative understeer.

To remedy the problem, the MPC should allow high rate of change of the yaw moment in extreme situations. Even though this approach will lead to higher torque disturbance, the sideslip angle will be minimized. An extra constraint terms must be added so that the stability of the vehicle prevails over the steering torque corruption. It could be done by using soft constraints on the sideslip angle and on the yaw moment rate instead of hard constraints. Therefore, the MPC problem is now:

$$\text{minimize } \mathcal{J} = \tilde{x}_{N_p}^T P \tilde{x}_{N_p} + \sum_{k=0}^{N_p-1} \tilde{x}_k^T Q_k \tilde{x}_k + \tilde{u}_k^T R \tilde{u}_k + \alpha_k R_\alpha \alpha_k + \gamma_k R_\gamma \gamma_k \tag{24}$$

$$\text{subject to } \tilde{x}_{k+1} = A\tilde{x}_k + B\tilde{u}_k \tag{25}$$

$$u_{min} \leq u_k \leq u_{max} \tag{26}$$

$$\Delta u_{min} - \alpha_k \leq u_k \leq \Delta u_{max} + \alpha_k \quad (27)$$

$$\beta_{min} - \gamma_k \leq \beta_k \leq \beta_{max} + \gamma_k \quad (28)$$

Parameters α_k and γ_k allows to infringe the constraint with a penalty cost. (26) limits the yaw moment according to the maximum torque the motors can provide. (27) limits the rate of the yaw moment and (28) limits the sideslip angle. The use of soft constraint on the sideslip angle ensures that the problem is feasible if the constraints cannot be enforced. In the following, $\max(Q, R) << R_\alpha < R_\gamma$ so that if all constrained are satisfied, the soft constraint on the rate of the yaw moment will be enforced. Moreover, the sideslip angle constraint prevails over the rate of the yaw moment minimization. The limit of the sideslip angle is set to 8° and soft constraint cost parameters are set to $R_\alpha = 20000/\Delta u_{max}^2$ and $R_\gamma = 50000/\beta_{max}^2$. The new MPC is tested on the same maneuver.

As shown by Figure 7, the MPC is able to maintain the sideslip angle within the prescribed range. The driver counter-steer less with the new controller than with the passive vehicle. The maximum rate of the yaw moment is not respected at the entry of the turn and at the middle of the turn to enforce the constraint on the sideslip angle instead.

VI. Conclusion

Front torque vectoring affect the steering torque felt by the driver in mechanically linked steering system. It adds a disturbance torque which can be approximated as proportional to the yaw moment. To prevent torque vectoring from disturbing the driver, the variation of the steering torque corruption has to be constrained. According to a neuromuscular model of the driver, what matters is not the amplitude of the torque disturbance but its rate: a human driver is able to reject large torque disturbance as long as it is slowly increased.

This constraint can be used in an MPC strategy. In this paper, the controller features a five degrees of freedom non-linear model. The rate of the torque disturbance is implemented by limiting the slew rate of the yaw moment. The limit value results trades-off between two contradictory goals: minimizing the disturbance and achieving high performance with fast response. Moreover, the MPC parameters also derived from compromises between computational burden and performance.

The controller has been tested in a high-simulation software (CarMaker). The MPC successfully limit the rate of the torque disturbance. However, in some situations, hard constraint on the yaw moment rate may be undesirable. For instance, when the vehicle is at the limit of lateral acceleration, a sudden drop in the yaw moment may be beneficial to have satisfactory understeer target following. Therefore, the use of soft constraint will help accomplish this task.

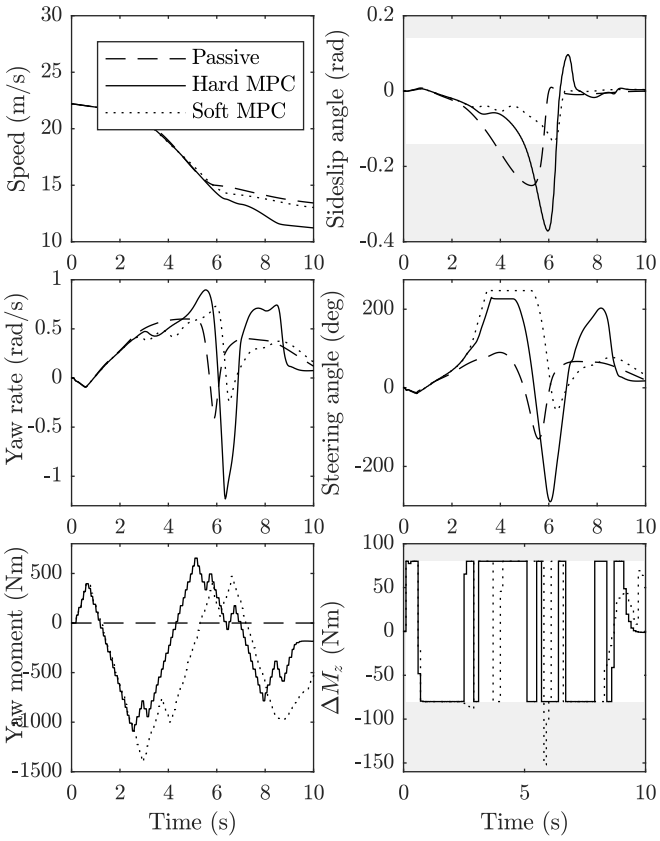

Fig. 7. Result from hairpin turn with soft and hard-constrained MPC. The dashed lines stand for the passive vehicle, the solid ones for the MPC which does not impose constraints on the sideslip angle and the dotted ones for the MPC with soft constraints on the yaw moment rate and the sideslip angle.

References

[1] L. De Novellis, et al. Comparison of feedback control techniques for torque-vectoring control of fully electric vehicles. IEEE Transactions on Vehicular Technology, 63(8):3612–3623, 2014.

[2] E. Siampis, E. Velenis, and S. Longo. Rear wheel torque vectoring model predictive control with velocity regulation for electric vehicles. Vehicle System Dynamics, 53(11):1555–1579, 2015.

[3] V. Scheuch, et al. A safe torque vectoring function for an electric vehicle. World Electric Vehicle Journal, 6(3):731–740, 2013.

[4] A. Neukum and H.-P. Krüger. Fahrerreaktionen bei lenksystemstrungen – untersuchungsmethodik und bewertungskriterien. VDI-Berichte Reifen – Fahrwerk – Fahrbahn, 1791:297–318, 2003.

[5] A. J. Pick and D. J. Cole. A mathematical model of driver steering control including neuromuscular dynamics. Journal of Dynamic Systems, Measurement, and Control, 130(3), 2008.

[6] J. Reimpell, et al. The automotive chassis: engineering principles. Butterworth-Heinemann, Würzburg, second edition, 2001.

[7] T. D. Gillespie. Fundamentals of Vehicle Dynamics. Society of Automotive Engineers, 1992.

[8] H. Pacejka. Tire and Vehicle Dynamics. Elsevier Ltd, 2012.

[9] W. Hoult and D. J. Cole. A neuromuscular model featuring co-activation for use in driver simulation. Vehicle System Dynamics, 46(sup1):175–189, 2008.

[10] D. A. Abbink, et al. Measurements of muscle use during steering wheel manipulation. Conference Proceedings - IEEE International Conference on Systems, Man and Cybernetics, 2011.

[11] R. S. Sharp and V. Valtetsiotis. Optimal preview car steering control. Vehicle System Dynamics Supplement, 35:101–117, 2001.

[12] J. P. Switkes, et al. Driver response to steering torque disturbances: a user study on assisted lanekeeping. IFAC Proceedings Volumes, 2007.

[13] L. De Novellis, et al. Design and comparison of the handling performance of different electric vehicle layouts. Proceedings of the Institution of Mechanical Engineers, Part D: Journal of Automobile Engineering, 228(0):218–232, 2013.

[14] A. Domahidi and J. Jerez. FORCES Professional. embotech GmbH (http://embotech.com/FORCES-Pro), July 2014.